

Interaction of a G protein with an activated receptor opens the interdomain interface in the alpha subunit

Ned Van Eps^{a,1}, Anita M. Preininger^{b,1}, Nathan Alexander^{c,1}, Ali I. Kaya^b, Scott Meier^b, Jens Meiler^{c,2}, Heidi E. Hamm^{b,2}, and Wayne L. Hubbell^{a,2}

^aJules Stein Eye Institute and Department of Chemistry and Biochemistry, University of California, Los Angeles, CA 90095-7008; ^bDepartment of Pharmacology, Vanderbilt University School of Medicine, Nashville, TN 37232-6600; and ^cDepartment of Chemistry, Vanderbilt University, Nashville, TN 37232-6600

Contributed by Wayne L. Hubbell, April 14, 2011 (sent for review March 12, 2011)

In G-protein signaling, an activated receptor catalyzes GDP/GTP exchange on the G_α subunit of a heterotrimeric G protein. In an initial step, receptor interaction with G_α acts to allosterically trigger GDP release from a binding site located between the nucleotide binding domain and a helical domain, but the molecular mechanism is unknown. In this study, site-directed spin labeling and double electron–electron resonance spectroscopy are employed to reveal a large-scale separation of the domains that provides a direct pathway for nucleotide escape. Cross-linking studies show that the domain separation is required for receptor enhancement of nucleotide exchange rates. The interdomain opening is coupled to receptor binding via the C-terminal helix of G_α , the extension of which is a high-affinity receptor binding element.

signal transduction | structural polymorphism

The α -subunit (G_α) of heterotrimeric G proteins ($G_{\alpha\beta\gamma}$) mediates signal transduction in a variety of cell signaling pathways (1). Multiple conformational states of G_α are involved in the signal transduction pathway shown in Fig. 1A. In the inactive state, the G_α subunit contains a bound GDP [$G_\alpha(\text{GDP})$] and has a high affinity for $G_{\beta\gamma}$. When activated by an appropriate signal, a membrane-bound G-protein coupled receptor (GPCR) binds the heterotrimer in a quaternary complex, leading to the dissociation of GDP and formation of an “empty complex” [$G_\alpha(0)_{\beta\gamma}$], which subsequently binds GTP. The affinity of $G_\alpha(\text{GTP})$ for $G_{\beta\gamma}$ is dramatically reduced relative to $G_\alpha(\text{GDP})$, resulting in functional dissociation of active $G_\alpha(\text{GTP})$ from the membrane-bound complex. The active $G_\alpha(\text{GTP})$ subsequently binds downstream effector proteins to trigger a variety of regulatory events, depending on the particular system. Thus, the GPCR acts to catalyze GDP/GTP exchange via an empty complex. Crystallographic (2–7), biochemical (8), and biophysical (9–11) studies have elucidated details of the conformational states of G_α that correspond to the discrete steps indicated in Fig. 1A, but the mechanism by which receptor interaction leads to release of the bound GDP from G_α and the structure of the empty complex remain a major target of research in the field.

The G_α subunit has two structural domains, namely a nucleotide binding domain and a helical domain that partially occludes the bound nucleotide (Fig. 1B). From the initial G_α crystal structure in 1993, Noel et al. (2) recognized that nucleotide release would probably require an opening between the two domains in the empty complex, but in the intervening 18 years there has been little compelling experimental support for this idea. Nevertheless, some constraints on the general topology of the complex are known. For example, numerous studies indicate that the C terminus of G_α is bound tightly to the receptor in the empty complex (9). In addition, the N-terminal helix of G_α is associated with $G_{\beta\gamma}$ and with the membrane via N-terminal myristoylation (12, 13). Together, these constraints fix the position of the nucleotide domain with respect to the membrane. The helical domain is connected to the nucleotide domain through two flexible linkers, and linker 1 (switch I) undergoes conformational changes upon

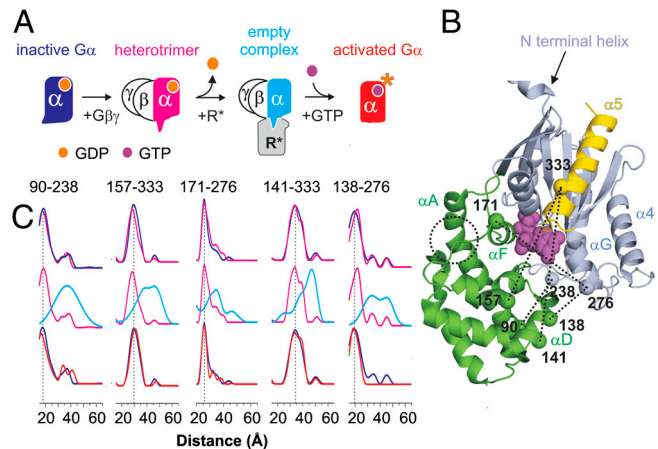


Fig. 1. Receptor activation of G proteins leads to a separation between domains. (A) The pathway of G_α activation via activated rhodopsin (R^*). The alpha subunit is color coded to denote the four different states investigated by SDSL/DEER spectroscopy. (B) Ribbon model of $G_{\alpha i}(\text{GDP})$ (PDB ID code 1GP2). The helical and nucleotide binding domains are colored green and light blue, respectively, and GDP is shown as magenta spheres. Relevant secondary structural elements are noted for reference. The C-terminal helix $\alpha 5$ is colored yellow; six disordered residues at the C terminus are not displayed. The N-terminal helix is truncated for convenience. Sites from which R1 nitroxide side chains were selected pair wise for distance measurements are indicated by spheres; dotted traces indicated specific distances measured for each state in A. (C) Distance distributions for the indicated doubly spin-labeled mutants. (Top) Compares $G_{\alpha i}(\text{GDP})$ and $G_{\alpha i}(\text{GDP})\beta\gamma$; (Middle) compares $G_{\alpha i}(\text{GDP})\beta\gamma$ and $R^* \cdot G_{\alpha i}(0)\beta\gamma$; (Lower) compares $G_{\alpha i}(\text{GDP})$ and $G_{\alpha i}(\text{GTP})$; traces are color coded to match states in A.

receptor binding (10). These observations provided the motivation to look for relative motion of the two G_α domains during formation of the empty complex.

For this purpose, site-directed spin labeling (SDSL) and double electron–electron resonance (DEER) spectroscopy were employed to measure distances between pairs of spin labels, with one label in each domain. Distances were measured for each state of G_α along the activation pathway using activated rhodopsin (R^*) as the GPCR. The results indicate that receptor-catalyzed nucleotide exchange in G proteins requires a large-scale reorientation of domains in the G protein α -subunit.

Author contributions: N.V.E., A.M.P., N.A., J.M., H.E.H., and W.L.H. designed research; N.V.E., A.M.P., N.A., A.I.K., and S.M. performed research; N.V.E., A.M.P., N.A., A.I.K., J.M., H.E.H., and W.L.H. analyzed data; and N.V.E., A.M.P., N.A., J.M., H.E.H., and W.L.H. wrote the paper.

The authors declare no conflict of interest.

¹N.V.E., A.M.P., and N.A. contributed equally to this work.

²To whom correspondence should be addressed. E-mail: jens.meiler@vanderbilt.edu, heidi.hamm@vanderbilt.edu, or hubbellw@jsei.ucla.edu.

This article contains supporting information online at www.pnas.org/lookup/suppl/doi:10.1073/pnas.1105810108/-DCSupplemental.

Results and Discussion

Using SDSL and DEER spectroscopy, distances were measured for each state of $G_{\alpha i}$ along the activation pathway using activated rhodopsin (R^*) as the GPCR. In these experiments, the R1 nitroxide side chain (Fig. S1) was introduced via cysteine substitution mutagenesis into the background of $G_{\alpha i}$ with reactive cysteines removed, HexaI ($G_{\alpha i}$ HI) (14). Fig. 1B shows the set of sites from which pairs were selected and the five specific interdomain distances investigated.

All doubly spin-labeled proteins bind to R^* to an extent similar to the $G_{\alpha i}$ HI parent protein as shown in direct endpoint binding assays (Fig. S2). In addition, they are all functional with respect to receptor-mediated nucleotide exchange, although mutants 138R1/276R1 and 157R1/333R1 have, respectively, about 40% and 55% of the receptor-catalyzed nucleotide exchange rate of the parent $G_{\alpha i}$ HI protein (Fig. S2). The reduced rates suggest that the residues involved are important in modulating receptor-mediated nucleotide exchange. In crystal structures of the inactive protein, residues Asn157 and Glu276 are involved in side chain H bonding and electrostatic interactions, respectively, and mutation of these may influence local conformation.

DEER spectroscopy relies on magnetic dipolar interactions between spin labels to measure interspin distances in the range of ≈ 17 – 60 Å (15, 16). Of particular importance is the ability to resolve multiple distances and the widths of the distributions. Fig. 1C compares the distance probability distributions for the five transdomain R1 pairs in each of the four states of $G_{\alpha i}$, i.e., $G_{\alpha i}(\text{GDP})$, $G_{\alpha i}(\text{GDP})_{\beta\gamma}$, $G_{\alpha i}(0)_{\beta\gamma}$, and $G_{\alpha i}(\text{GTP})$. For each pair, the measured most probable distances for $G_{\alpha i}(\text{GDP})$ and $G_{\alpha i}(\text{GDP})_{\beta\gamma}$ agree well with expectations from the crystal structures (5–7) and models of the R1 side chain (17). In all cases there is little difference between $G_{\alpha i}(\text{GDP})$ and $G_{\alpha i}(\text{GDP})_{\beta\gamma}$.

Upon photoactivation of rhodopsin and formation of the $R^* \cdot G_{\alpha i}(0)_{\beta\gamma}$ complex, there is a remarkable increase in each interspin distance, with increases being as large as 20 Å (at 90/238) (for details, see *SI Text* and Figs. S3 and S4). Moreover, there is a dramatic increase in width of each distribution as well as multiple distances in most cases. It is of interest that distances present in the $G_{\alpha i}(0)_{\beta\gamma}$ distributions correspond approximately to minor populations already present in $G_{\alpha i}(\text{GDP})$ and $G_{\alpha i}(\text{GDP})_{\beta\gamma}$, suggesting that activation may shift an existing equilibrium. Although the exact widths of the distributions in $G_{\alpha i}(0)_{\beta\gamma}$ may not be well-determined in each case, they are clearly broader than possible from multiple rotamers of R1, suggesting spatial disorder of the G_{α} protein in the empty-pocket state of the activated complex (see *SI Text*). Finally, addition of $\text{GTP}\gamma\text{S}$ restores a state with a most probable distance and width of distribution similar to the GDP bound state. This is in agreement with expectations from $\text{GTP}\gamma\text{S}$ bound crystal structures (6).

The EPR spectra of R1 residues at the sites shown in Fig. 1B have little or no changes upon receptor activation (Fig. 2). This result, taken together with the very large distance changes observed, ensure that the detected distance increases reflect global domain movement rather than simple R1 side chain rearrangements due to changes in local environment. Collectively, the data strongly support a model for a $G_{\alpha i}(0)_{\beta\gamma}$ in which the helical domain is displaced relative to the nucleotide domain in the heterotrimer, and in which the structure is highly flexible with respect to the relative domain orientations.

To visualize the domain opening, a model of the empty complex on the receptor was constructed that is consistent with the DEER and other available experimental data (see *SI Text*). To generate the model, the heterotrimeric G_i was docked with the photoreceptor using crystal structures of $G_{\alpha i}(\text{GDP})_{\beta\gamma}$ (4, 7) and opsin in complex with the high-affinity G_{α} C-terminal peptide (18). The $G_{\alpha i}$ C-terminal helix was fused with the high-affinity G_{α} C-terminal peptide bound to opsin (for details, see *SI Text* and Figs. S5 and S6), which provided a convenient starting

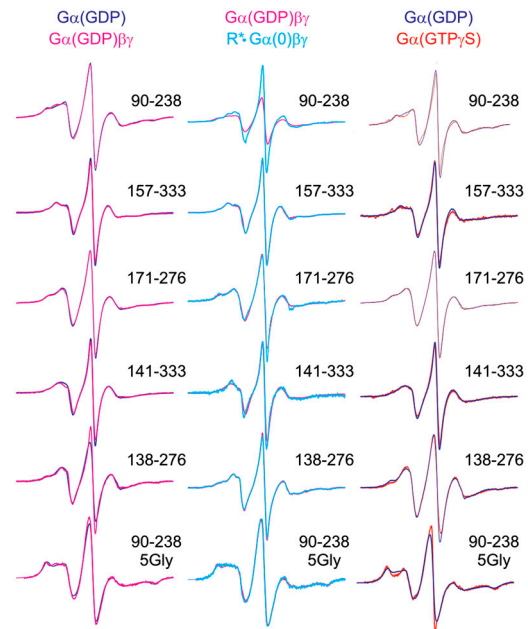


Fig. 2. CW EPR spectra of the spin-labeled double mutants in $G_{\alpha i}$ at the indicated states along the activation pathway. (Left) Compares EPR spectra of the doubly labeled $G_{\alpha i}(\text{GDP})$ and $G_{\alpha i}(\text{GDP})_{\beta\gamma}$ mutants; (Middle) compares $G_{\alpha i}(\text{GDP})_{\beta\gamma}$ and $R^* \cdot G_{\alpha i}(0)_{\beta\gamma}$; (Right) compares $G_{\alpha i}(\text{GDP})$ and $G_{\alpha i}(\text{GTP})$.

point for the model (19). The myristoylated N-terminal amphipathic helix was placed parallel to the membrane surface and the heterotrimer oriented such that both the myristoyl group and the nearby farnesylated C terminus of the G_{γ} -subunit can be inserted into the membrane; together these hydrophobic interactions cooperatively drive membrane binding of the intact heterotrimer (20). The procedure required chain breaks within the linker regions of the α -subunit (between residues 59–60 and 184–185) and resulted in clashes in loop regions within the heterotrimer that were then resolved through loop reconstruction and model relaxation in Rosetta (21, 22). A rigid body docking protocol was executed to find placements of the helical domain consistent with the DEER distance restraints (*SI Text*, Fig. S7, and Table S1). An ensemble of models was found to be in agreement with the experimental distances from DEER data, consistent with the increase in width of the distance distributions (Fig. S8). The model that agrees best with the most probable distances from DEER data (Fig. 3B) fulfills all distance restraints within the error of the experiment and involves an approximately 8-Å motion of the helical domain away from the nucleotide

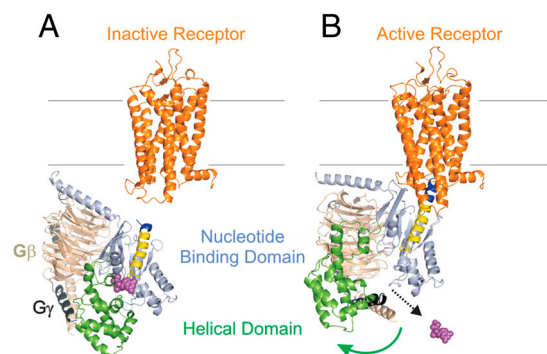


Fig. 3. A model showing the opening of the interdomain cleft in formation of the empty complex. (A) The inactive receptor (1U19.pdb) and inactive G protein (see *SI Text*), with color coding as in Fig. 1. (B) Model of the complex with active receptor (3DQB.pdb) showing the reorientation of the helical domain (Movie S1).

residues in the R90C-E238C protein, based on the predicted proximity between these thiols in the $G_{\alpha i}$ (GDP) protein (Fig. 5A). Cross-linking resulted in a $G_{\alpha i}$ (GDP) $\beta\gamma$ -protein competent to bind activated receptors to approximately the same extent as the parent protein (Fig. 5B). Moreover, the cross-linked protein undergoes aluminum fluoride-dependent conformational changes (Fig. 5C, *Inset*) consistent with an active, properly folded protein. On the other hand, this protein exhibited severely impaired rates of receptor-mediated nucleotide exchange as compared to either the parent or uncross-linked protein (Fig. 5C), demonstrating the essential nature of the domain separation in receptor-mediated G-protein activation. The basal nucleotide exchange rate was only slightly reduced (Fig. 5C), suggesting an effect specific to receptor-mediated nucleotide release, the slow step in G-protein activation.

Conclusions

This study demonstrates that the result of G-protein interaction with an activated receptor is propagated allosterically to reorient the distant helical domain of $G_{\alpha i}$, opening the domain interface in formation of a flexible ternary receptor–G-protein complex. Preventing the large interdomain movement through cross-linking markedly reduces the rate of catalyzed nucleotide exchange, demonstrating the crucial role of the interdomain opening in receptor-mediated G-protein activation. Although the detailed mechanism is currently under further investigation, this domain opening would be predicted to reduce the GDP binding energy as interactions are lost upon opening of the domain interface. Together these changes help broaden our understanding of the conformational changes in the G protein that lead to GDP release, the slow step in G-protein activation.

Methods

Membrane Binding Assays. The ability of wild-type and $G_{\alpha i}$ proteins containing the side chain R1 (Fig. S1) to bind rhodopsin was tested as described previously (31). For additional details, see *SI Methods*.

Cross-Linking. The bifunctional cross-linking reagent 1,11-bis(maleimido) triethylene glycol (Pierce Biotechnology) was incubated in a 2:1 molar ratio with $G_{\alpha i}$ Hexa I-R90C-E238C at 4 °C for 2 h in 50 mM Tris, 130 mM NaCl, 10 mM $MgCl_2$, 5 mM EDTA, 100 μ M GDP, at pH 7.0. After 2 h, reaction was quenched with chromatography buffer (50 mM Tris, 130 mM NaCl, 2 mM $MgCl_2$, 10 μ M GDP, 1 μ M EDTA, 1 mM DTT, pH 7.5) and concentrated in this buffer. The concentrated, cross-linked monomeric protein was then purified by gel filtration FPLC on a calibrated SW2000 column (Sigma). Calibration was performed under the same conditions as purification, using a broad range of molecular weight standards (Biorad).

Nucleotide Exchange Assays. G proteins and rod outer segment (ROS) membranes were prepared essentially as previously described (10). The rates of basal and receptor-mediated nucleotide exchange of the spin-labeled G_{α} proteins were measured at excitation/emission wavelengths of 290/340 nm in buffer containing 50 mM Tris, 130 mM NaCl, 2 mM $MgCl_2$, 1 mM DTT, 1 μ M EDTA, pH 7.5, for 40 min at 18 °C after addition of 10 μ M GTP γ S. For receptor-stimulated exchange, proteins were reconstituted with an equimolar amount of $G_{\beta\gamma 1}$ (200 nM each) prior to measurement of exchange; the experiments were performed in the presence of light activated rhodopsin (100 nM) obtained from urea washed ROS membranes. Basal exchange was carried out in the absence of rhodopsin and $G_{\beta\gamma}$. The data were normalized to

the baseline and the fluorescence maximum, and rate of exchange was determined by fitting the data to an exponential association curve. Rates shown in Fig. S2B are from a minimum of four independent experiments (\pm SEM).

Spin Labeling and Electron Paramagnetic Resonance Measurements. Spin labeling was carried out in buffer containing 20 mM 3-(N-morpholino)propane-sulfonic acid (pH 6.8), 100 mM NaCl, 2 mM $MgCl_2$, 50 μ M GDP, and 10% glycerol (vol/vol). The $G_{\alpha i}$ double mutants were incubated with the sulfhydryl spin-label S-(1-oxy-2,2,5,5-tetramethylpyrroline-3-methyl)-methanethiosulfonate in a 2:1 molar ratio at room temperature for 5 min. Noncovalently bound nitroxide was removed by extensive washing with labeling buffer using a 30-kDa molecular weight concentrator.

A series of EPR spectra were recorded for each spin-labeled mutant. Continuous wave (CW) EPR spectra were recorded at room temperature on a Bruker E580 spectrometer using a high-sensitivity resonator (HS0118) at X-band microwave frequencies. Each spectrum was collected using a 100-G field scan at a microwave power of 19.92 mW. Optimal field-modulation amplitudes were selected to give maximal signal intensity without line-shape distortion. The data were typically averages of approximately 20 scans.

Four-Pulse DEER Measurements. The spin-labeled proteins were flash frozen within quartz capillaries in a liquid nitrogen bath. After freezing, they were loaded into a 2-mm split-ring resonator, and DEER measurements were performed at 80 K on a Bruker Elexsys 580 spectrometer. Four-pulse DEER was carried out as previously described (32), with the π -pump pulse (16 ns) was positioned at the absorption maximum of the field swept nitroxide center line and the observer π (16 ns) and $\pi/2$ (8 ns) pulses at the absorption maximum of the low-field line.

The buffer used for DEER measurements was similar to the CW EPR experiments. Four different states of each double-labeled mutant were measured to determine conformational changes along the G-protein activation pathway. All DEER data were analyzed with the DEER Analysis 2011 software package freely available at the Web site <http://www.epr.ethz.ch/>, and with a Labview software package provided by Christian Altenbach (Jules Stein Eye Institute, Los Angeles, CA). Details for utilization of the DEER Analysis 2011 software package were previously described (33). Background correction of the primary dipolar evolution data was performed as described (33). For distance distributions below 20 Å, excitation bandwidth corrections were applied (34). These corrections had very little effect on the computed distributions. Tikhonov regularization techniques were used for fitting the data using L-curve methods for determining the regularization parameter (35). In some instances, Gaussian fitting was also employed where distribution widths of the Gaussian fits were guided by Tikhonov results. Figs. S3 and S4 show the background-corrected dipolar evolution data, the dipolar spectra, and the normalized integral representations of the distance distributions. For the distances between the nucleotide and helical domains in the receptor-bound empty complex, the width of the distribution may not be well determined due to the limited collection time of the dipolar evolution. Nevertheless, the fact that the distribution is indeed broad is revealed by the lack of well-defined oscillations in the dipolar evolution.

Modeling of the Complex Based on Available Information, Including DEER Distances. For details about the modeling of the complex, see *SI Methods*.

ACKNOWLEDGMENTS. The authors gratefully acknowledge helpful discussions with C. Altenbach and thank C. Hubbell, C. J. López, V. V. Gurevich, and C. R. Sanders for carefully reading the manuscript. Research reported here was supported by National Institutes of Health Grants GM080403 (to J.M.), EY006062 (to H.E.H.), EY005216 (to W.L.H.) and the Jules Stein Professorship endowment (to W.L.H.). N.A. was supported by National Research Service Award MH086222.

1. Tesmer JJ (2010) The quest to understand heterotrimeric G protein signaling. *Nat Struct Mol Biol* 17:650–652.
2. Noel JP, et al. (1993) The 2.2 Å crystal structure of transducin- α complexed with GTP γ S. *Nature* 366:654–663.
3. Lambright DG, et al. (1994) Structural determinants for activation of the α -subunit of a heterotrimeric G protein. *Nature* 369:621–628.
4. Lambright DG, et al. (1996) The 2.0 Å crystal structure of a heterotrimeric G protein. *Nature* 379:311–319.
5. Coleman DE, et al. (1998) Crystal structures of the G protein Gi α 1 complexed with GDP and Mg^{2+} : A crystallographic titration experiment. *Biochemistry* 37:14376–14385.
6. Coleman DE, et al. (1994) Structures of active conformations of Gi α 1 and the mechanism of GTP hydrolysis. *Science* 265:1405–1412.
7. Wall MA, et al. (1995) The structure of the G protein heterotrimer Gi α 1 β 1 γ 2. *Cell* 83:1047–1058.
8. Higashijima T, et al. (1987) Effects of Mg^{2+} and the β γ -subunit complex on the interactions of guanine nucleotides with G proteins. *J Biol Chem* 262:762–766.
9. Oldham WM, et al. (2006) Mechanism of the receptor-catalyzed activation of heterotrimeric G proteins. *Nat Struct Mol Biol* 13:772–777.
10. Oldham WM, et al. (2007) Mapping allosteric connections from the receptor to the nucleotide-binding pocket of heterotrimeric G proteins. *Proc Natl Acad Sci USA* 104:7927–7932.
11. Van Eps N, et al. (2006) Structural and dynamical changes in an α -subunit of a heterotrimeric G protein along the activation pathway. *Proc Natl Acad Sci USA* 103:16194–16199.

12. Linder ME, et al. (1991) Lipid modifications of G protein subunits. Myristoylation of Go alpha increases its affinity for beta gamma. *J Biol Chem* 266:4654–4659.
13. Resh MD, et al. (1999) Fatty acylation of proteins: New insights into membrane targeting of myristoylated and palmitoylated proteins. *Biochim Biophys Acta* 1451:1–16.
14. Medkova M, et al. (2002) Conformational changes in the amino-terminal helix of the G protein alpha(i1) following dissociation from Gbetagamma subunit and activation. *Biochemistry* 41:9962–9972.
15. Pannier M, et al. (2000) Dead-time free measurement of dipole-dipole interactions between electron spins. *J Magn Reson* 142:331–340.
16. Jeschke G (2002) Distance measurements in the nanometer range by pulse EPR. *Chemphyschem* 3:927–32.
17. Fleissner MR, et al. (2009) Structural origin of weakly ordered nitroxide motion in spin-labeled proteins. *Protein Sci* 18:893–908.
18. Scheerer P, et al. (2008) Crystal structure of opsin in its G-protein-interacting conformation. *Nature* 455:497–502.
19. Scheerer P, et al. (2009) Structural and kinetic modeling of an activating helix switch in the rhodopsin-transducin interface. *Proc Natl Acad Sci USA* 106:10660–10665.
20. Hermann R, et al. (2006) Signal transfer from GPCRs to G proteins: Role of the G alpha N-terminal region in rhodopsin-transducin coupling. *J Biol Chem* 281:30234–30241.
21. Kaufmann KW, et al. (2010) Practically useful: What the Rosetta protein modeling suite can do for you. *Biochemistry* 49:2987–2998.
22. Hirst SJ, et al. (2011) RosettaEPR: An integrated tool for protein structure determination from sparse EPR data. *J Struct Biol* 173:506–514.
23. Preininger AM, et al. (2009) Helix dipole movement and conformational variability contribute to allosteric GDP release in G α_i subunits. *Biochemistry* 48:2630–2642.
24. Hamm HE, et al. (1988) Site of G protein binding to rhodopsin mapped with synthetic peptides from the alpha subunit. *Science* 241:832–835.
25. Marin EP, et al. (2002) Disruption of the alpha5 helix of transducin impairs rhodopsin-catalyzed nucleotide exchange. *Biochemistry* 41:6988–6994.
26. Martin EL, et al. (1996) Potent peptide analogues of a G protein receptor-binding region obtained with a combinatorial library. *J Biol Chem* 271:361–366.
27. Dratz EA, et al. (1993) NMR structure of a receptor-bound G-protein peptide. *Nature* 363:276–281.
28. Kisselev OG, et al. (1998) Light-activated rhodopsin induces structural binding motif in G protein alpha subunit. *Proc Natl Acad Sci USA* 95:4270–4275.
29. Van Eps N, et al. (2010) Electron paramagnetic resonance studies of functionally active, nitroxide spin-labeled peptide analogs of the C-terminus of a G-protein alpha subunit. *Biochemistry* 49:6877–6886.
30. Natochin M1, et al. (2001) Probing the mechanism of rhodopsin-catalyzed transducin activation. *J Neurochem* 77:202–210.
31. Preininger AM, et al. (2008) Receptor-mediated changes at the myristoylated amino terminus of G α_{i1} proteins. *Biochemistry* 47:10281–10293.
32. Hanson SM, et al. (2007) Structure and function of the visual arrestin oligomer. *EMBO J* 26:1726–1736.
33. Jeschke G, et al. (2006) DeerAnalysis2006: A comprehensive software package for analyzing pulsed ELDOR. *Appl Magn Reson* 30:473–498.
34. Banham JE, et al. (2008) Distance measurements in the borderline region of applicability of CW EPR and DEER: A model study on a homologous series of spin-labeled peptides. *J Magn Reson* 191:202–218.
35. Chiang YW, et al. (2005) The determination of pair distance distributions by pulsed ESR using Tikhonov regularization. *J Magn Reson* 172:279–295.

Supporting Information

Van Eps et al. 10.1073/pnas.1105810108

SI Methods.

Membrane Binding Assays.

$G_{\alpha i}$ (5 μ M) subunits were preincubated with $G_{\beta\gamma}$ (10 μ M) subunits on ice for 10 min. Then, in the dark, rhodopsin (50 μ M) within native membranes was added to the heterotrimeric G protein in a buffer containing 50 mM Tris (pH 8.0), 100 mM NaCl, 1 mM $MgCl_2$ and incubated on ice for 5 min. For dark measurements, reaction mixtures were protected from light for the rest of the procedure. Light activated samples, as well as light activated samples with GTP γ S (100 μ M), were incubated on ice for 30 min. The membranes in each treatment (dark, light, and light plus GTP γ S) were pelleted by centrifugation at $20,000 \times g$ for 1 h at 4 °C, and supernatants were removed from pellets. For the dark samples, supernatants were removed under dim red light. The supernatants and pellets of each treatment were boiled and resolved by SDS-PAGE. The protein samples were visualized with Coomassie blue and quantified by densitometry using a BioRad Multimager. Each sample was evaluated by comparison of the amount of $G_{\alpha i}$ subunits in pellet (P) or supernatant (S) to the total amount of $G_{\alpha i}$ subunits (P+S) in both treatments and expressed as a percentage of the total $G_{\alpha i}$ protein. Results are averages from at least three independent experiments. Results are shown in Fig. S2A.

Modeling of the Complex Based on Available Information, Including DEER Distances.

Comparative Model of the Heterotrimeric G-Protein Transducin with $G_{\alpha i}$ Sequence. The structure of the heterotrimeric G-protein transducin (PDB ID code 1GOT) was used as a template. The heterotrimeric protein consists of three subunits, α , β , and γ , and has GDP bound. The α -subunit (chain A) of the protein is a chimera of $G_{\alpha t}$ of bovine and $G_{\alpha i}$ of rat. A comparative model was constructed that consists entirely of the $G_{\alpha i}$ rat sequence using the sequence alignment shown in Fig. S5. The sequence alignment shows an extension of the N-terminal α -helix by one winding (four-residue gap) that was built in the comparative model as a straight α -helix. The Rosetta side chain construction algorithm (1) was then used to convert the appropriate residues of 1GOT into $G_{\alpha i}$ sequence, yielding a comparative model termed $G_{\alpha i}$ -1GOT. The command line options used are shown below:

```
fixbb.linuxgccrelease -database -in:file:s -out:file:fullatom -resfile -out:prefix
```

Superposition of the Transducin C-Terminal Helix with the Opsin-Bound Peptide Ligand. The structure of G-protein coupled receptor opsin in complex with the C-terminal 11 residues of the α -subunit of the G-protein heterotrimer (PDB ID code 3DQB) was fused with the comparative model $G_{\alpha i}$ -1GOT. Specifically, residues 344–347 in the α -subunit of the $G_{\alpha i}$ -1GOT structure overlap in sequence with the first four residues of the peptide ligand in 3DQB (Fig. S6). Using these four overlapping residues, the heterotrimer was positioned relative to the receptor. This defines an initial position of the heterotrimer relative to the receptor. As already described by Scheerer et al. (2), this procedure positions portions of the heterotrimer in the membrane core in a nonphysical way.

In order to resolve the penetration of the heterotrimer into the membrane core, rotations of portions of the heterotrimer are performed at two pivot points. Subunits β and γ are rotated

along with the N-terminal helix and switch-2 region of the α -subunit such that the resulting position of the N-terminal helix is approximately parallel with the membrane (40° rotation). A second rotation of 15° of the heterotrimer is applied at the junction of the 3DQB peptide and C-terminal helix of $G_{\alpha i}$ -1GOT, moving the N-terminal helix parallel with the membrane.

The combination of these two rotations creates a physically realistic model that removes the β -, γ -subunits from the membrane core, places the N-terminal amphipathic helix parallel to the membrane surface, and puts the N terminus in a location that allows the alkyl chain of the myristoyl group and the nearby farnesylated C terminus of the γ -subunit to penetrate the membrane. The procedure results in chain breaks within the α -subunit and minor clashes in loop regions within the heterotrimer that are resolved via the Rosetta loop building protocol.

α -Helical Domain Docking. EPR distance measurements display a reorientation of the helical domain of the α -subunit when the heterotrimer binds to the receptor (Fig. 1). In order to capture this conformational motion, the α -helical domain was detached from the rest of the α -subunit by introduction of chain breaks between residues 59/60 and 184/185 of chain A of the $G_{\alpha i}$ -1GOT structure. Next, a rigid body docking protocol was executed to sample possible placements of the helical domain with respect to the α -subunit. A total of 140,000 structures were created using Rosetta (3). The starting position of the α -helical domain was initially perturbed by up to 1.5 Å and 4° rotation. During docking trajectories translations of up to 0.05 Å and rotations of up to 2.5° were performed in a stepwise procedure. The command line flags used follow:

```
docking_protocol.linuxgccrelease -in:file:s start.pdb -out:nstruct 100 -docking:dock_pert 1.5 4 -docking:dock_mcm_trans_magnitude 0.05 -docking:dock_mcm_rot_magnitude 2.5 -out:overwrite
```

Filtering of α -Helical Domain Docking Models. Docking models were filtered for agreement with EPR distance data after docking. Agreement with the EPR distance restraints is calculated according to the knowledge-based potential given by Hirst et al. (4). Agreement can be expressed with a value between 0 (no agreement) and -1 (perfect agreement, Fig. S7A). In addition to the EPR distances, a filter was applied to ensure the chain break created at the cut points can be resolved through remodeling a minimal number of residues around the cut points. This filter minimizes the distances between residues 59/60 and 184/185 of the α -subunit of $G_{\alpha i}$ -1GOT (Fig. S7B). The 1,000 models that pass both filters undergo a clustering analysis (Fig. S8), and the cluster center that agrees best with the experimental data is used for all further analysis (Table S1). This model shows a translation of approximately 8 Å and a rotation of 29° of the α -helical domain compared to its starting position.

The increased width in the distance distributions obtained from EPR spectroscopy (Fig. 1C) suggests a flexible relative orientation of the helical domain with respect to the heterotrimer in the receptor-bound state. The ensemble of 1,000 models in agreement with the EPR data might reflect part of this spatial disorder. A single model was selected to facilitate discussion of the general movement of the α -helical domain, as it is consistent between all models (Figs. S8 and S9). We conclude that this movement is well defined by the experimental data. Additional experimental measurements will be necessary to determine the parameters of the spatial disorder.

Rosetta loop building (5) and relaxation protocols (6) were utilized in order to reconnect the helical domain back to the rest of the α -subunit and refine the complex within the Rosetta energy functions. In addition, the α A helix (α -subunit residues 63–90)

is unlinked in the model of the activated heterotrimer–receptor complex solely for demonstrative purposes of a possible mechanism of leverage for generating the helical domain movement (see main article).

1. Kuhlman B, et al. (2003) Design of a novel globular protein fold with atomic-level accuracy. *Science* 302:1364–1368.
2. Scheerer P, et al. (2008) Crystal structure of opsin in its G-protein-interacting conformation. *Nature* 455:497–502.
3. Gray JJ, et al. (2003) Protein-protein docking with simultaneous optimization of rigid-body displacements and side-chain conformations. *J Mol Biol* 331:281–299.
4. Hirst SJ, Alexander N, McHaourab HS, Meiler J (2011) An integrated tool for protein structure determination from sparse EPR data. *J Struct Biol* 173:506–514
5. Wang C, Bradley P, Baker D (2007) Protein-protein docking with backbone flexibility. *J Mol Biol* 373:503.
6. Misura KMS, Baker D. (2005) Progress and challenges in high-resolution refinement of protein structure models. *Proteins* 59:15–29.

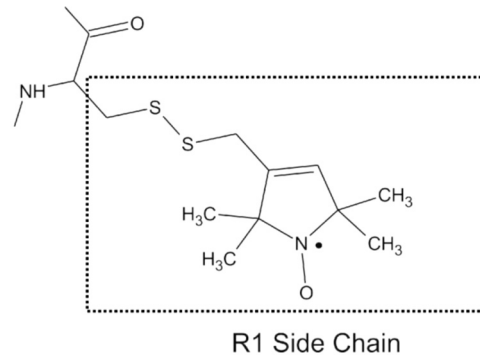


Fig. S1. The nitroxide R1 side chain.

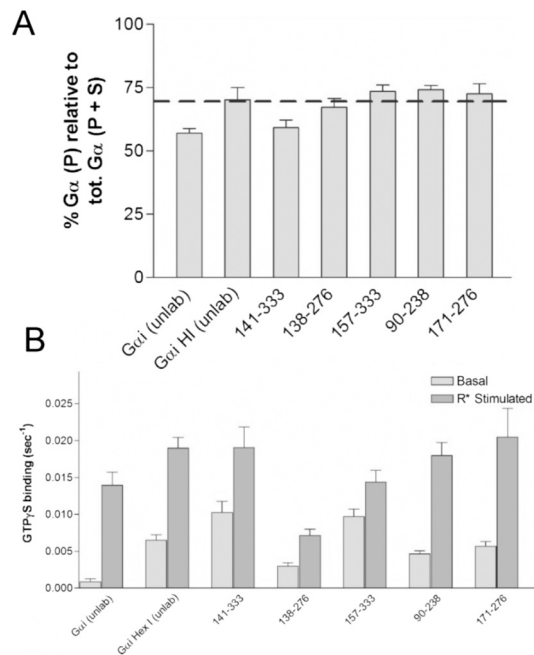
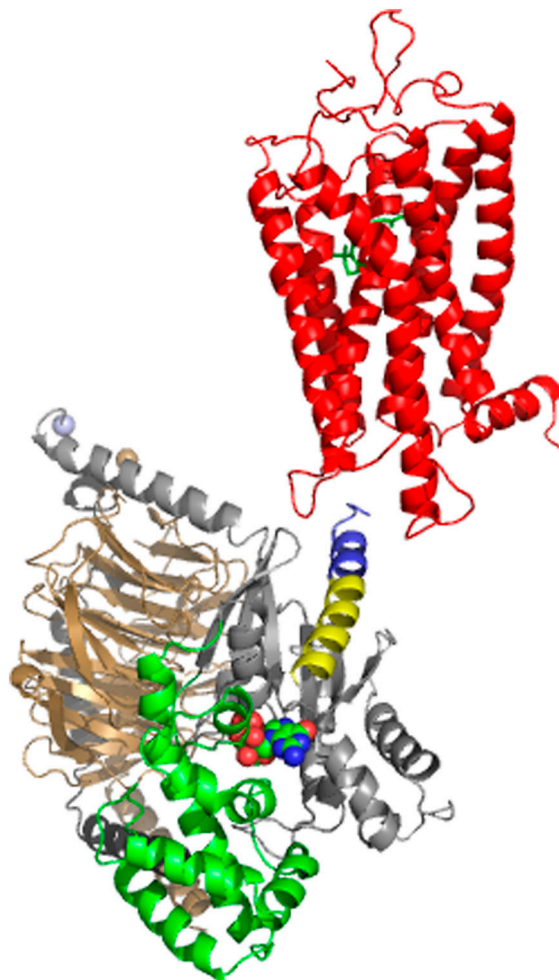


Fig. S2. (A) Binding of doubly spin-labeled mutants to rhodopsin in disc membranes. (B) Basal and receptor catalyzed nucleotide exchange rates for the doubly spin-labeled mutants. Assays were performed as described in *Methods*.



Movie S1. Animation showing the hypothesized conformational changes leading to GDP release. The crystal structure of rhodopsin before activation [red, PDB ID code 1U19 (1)] transitions to the activated state [orange, R*, PDB ID code 3DQB (2)]. The GDP-bound heterotrimer binds to R* and the helical domain of $G_{\alpha}(GDP)$ opens away from the nucleotide binding domain. The opening movement allows GDP release leading to $G_{\alpha}(0)_{\beta\gamma}$. Color scheme is $G_{\beta\gamma}$, tan; G_{γ} , black; $G_{\alpha}(GDP)$ helical domain, green; $G_{\alpha}(GDP)$ nucleotide binding domain, gray; GDP, spheres. The animation was created using Pymol RigiMOL (Schrodinger, LLC). [Movie S1 \(MOV\)](#)

- Okada T, et al. (2004) The retinal conformation and its environment in rhodopsin in light of a new 2.2 Å crystal structure. *J Mol Biol* 342:571–583.
- Scheerer P, et al. (2008) Crystal structure of opsin in its G-protein-interacting conformation. *Nature* 455:497–502.

Table S1. Agreement of the receptor-bound $G_{\alpha i}$ -1GOT model with experimentally measured EPR distances

Mutant:	90/238	157/333	171/276	141/333	138/276
EPR experiment:					
Free heterotrimer	18 Å	28 Å	26 Å	33 Å	20 Å
Bound to activated receptor	38 Å	45 Å	34 Å	46 Å	34 Å
Distance change	20 Å	17 Å	8 Å	13 Å	14 Å
Structures:					
Free heterotrimer	11 Å	25 Å	23 Å	32 Å	16 Å
Bound to activated receptor	32 Å	40 Å	25 Å	41 Å	29 Å
Distance change	21 Å	15 Å	2 Å	9 Å	13 Å
Agreement between experiment and model according to KBP	-0.96	-0.96	-0.71	-0.96	-0.97

The EPR distances in the table are determined from the most probable distances in each distribution. The distances measured in models are measured between C_{β} atoms. Distances for the free heterotrimer were calculated using the experimental crystal structure (PDB ID code 1GOT). Distances for the receptor-bound state were calculated using the $G_{\alpha i}$ -1GOT model. Distance agreement between the receptor-bound model and the EPR measurements were calculated according to the knowledge-based scoring potential (KBP) (4). Perfect agreement would be -1.0 and no agreement would be 0.0.